AGU PUBLICATIONS

JGR

Journal of Geophysical Research: Biogeosciences

RESEARCH ARTICLE
10.1002/2016JG003434

Key Points:
- Vapor pressure deficit explained fire variability at a level similar to fire weather indexes
- Tower CO, CH_4, and CO_2 measurements were used to determine fire emission factors
- The modeling system we developed may provide insight about emissions from individual Alaskan fires

Correspondence to:
E. B. Wiggins,
wigginse@uci.edu

Citation:
Wiggins, E. B., et al. (2016), The influence of daily meteorology on boreal fire emissions and regional trace gas variability, *J. Geophys. Res. Biogeosci.*, *121*, 2793–2810, doi:10.1002/2016JG003434.

Received 29 MAR 2016
Accepted 30 SEP 2016
Accepted article online 6 OCT 2016
Published online 18 NOV 2016

The influence of daily meteorology on boreal fire emissions and regional trace gas variability

E. B. Wiggins[1], S. Veraverbeke[1,2], J. M. Henderson[3], A. Karion[4,5], J. B. Miller[4], J. Lindaas[6], R. Commane[6], C. Sweeney[7], K. A. Luus[8], M. G. Tosca[9], S. J. Dinardo[9], S. Wofsy[6], C. E. Miller[9], and J. T. Randerson[1]

[1]Department of Earth System Science, University of California, Irvine, California, USA, [2]Faculty of Earth and Life Sciences, Vrije Universiteit Amsterdam, Amsterdam, Netherlands, [3]Atmospheric and Environmental Research, Inc., Lexington, Massachusetts, USA, [4]National Oceanic and Atmospheric Administration, Boulder, Colorado, USA, [5]Now at the National Institute of Standards and Technology, Gaithersburg, Maryland, USA, [6]School of Engineering and Applied Sciences, Harvard, Cambridge, Massachusetts, USA, [7]Cooperative Institute for Research in Environmental Sciences, University of Colorado Boulder, Boulder, Colorado, USA, [8]Centre for Applied Data Analytics, Dublin Institute of Technology, Dublin, Ireland, [9]Jet Propulsion Laboratory, California Institute of Technology, Pasadena, California, USA

Abstract Relationships between boreal wildfire emissions and day-to-day variations in meteorological variables are complex and have important implications for the sensitivity of high-latitude ecosystems to climate change. We examined the influence of environmental conditions on boreal fire emissions and fire contributions to regional trace gas variability in interior Alaska during the summer of 2013 using two types of analysis. First, we quantified the degree to which meteorological and fire weather indices explained regional variability in fire activity using four different products, including active fires, fire radiative power, burned area, and carbon emissions. Second, we combined daily emissions from the Alaskan Fire Emissions Database (AKFED) with the coupled Polar Weather Research and Forecasting/Stochastic Time-Inverted Lagrangian Transport model to estimate fire contributions to trace gas concentration measurements at the Carbon in Arctic Reservoirs Vulnerability Experiment-NOAA Global Monitoring Division (CRV) tower in interior Alaska. Tower observations during two high fire periods were used to estimate CO and CH_4 emission factors. We found that vapor pressure deficit and temperature had a level of performance similar to more complex fire weather indices. Emission factors derived from CRV tower measurements were 134 ± 25 g CO per kg of combusted biomass and 7.74 ± 1.06 g CH_4 per kg of combusted biomass. Predicted daily CO mole fractions from AKFED emissions were moderately correlated with CRV observations ($r = 0.68$) and had a high bias. The modeling system developed here allows for attribution of emission factors to individual fires and has the potential to improve our understanding of regional CO, CH_4, and CO_2 budgets.

1. Introduction

Boreal forest fires are an important driver of ecosystem dynamics, carbon balance, and climate feedbacks in the Northern Hemisphere [*Johnson*, 1996; *Turetsky et al*., 2015]. At a landscape scale, fires influence the age structure of forests, with postfire succession modifying species composition over a period of many decades [*Viereck et al*., 1983; *Wirth et al*., 1999]. Within individual burns, environmental conditions at the time of the fire can modify fire severity, and ultimately the recruitment and composition of vegetation that establishes in early successional stages [*Johnstone et al*., 2004; *Johnstone and Chapin*, 2006]. Boreal ecosystems are carbon rich, with accumulation rates enhanced by cold temperatures and slow decomposition rates [*Apps et al*., 1993; *Trumbore and Harden*, 1997; *Harden et al*., 2000; *Hobbie et al*., 2000; *McGuire et al*., 2010]. Much of this carbon is contained in organic soil layers that are vulnerable to fire [*Apps et al*., 1993; *Rapalee et al*., 1998] and account for 80–90% of the carbon released during combustion [*Boby et al*., 2010; *Turetsky et al*., 2011; *Rogers et al*., 2015]. A change in fire regime thus has the potential to influence radiative forcing by means of several different pathways, including modification of surface biophysics [*Amiro et al*., 2006; *Rogers et al*., 2013], terrestrial carbon stocks [*Harden et al*., 2000; *Turetsky et al*., 2011], and emissions of black carbon [*Martin et al*., 2006; *Preston and Schmidt*, 2006; *Flanner et al*., 2007; *Akagi et al*., 2011]. To reduce uncertainties in fire-climate feedbacks and allow more accurate prediction of future change, more information is needed to understand how meteorological factors influence the amount and composition of pyrogenic emissions.

Weather and climate strongly influence fire dynamics in boreal forests on time scales of hours to decades [*Johnson*, 1996]. Ambient weather conditions control lightning ignition probability [*Latham and Schlieter*,

1989; *Nash and Johnson*, 1996; *Anderson*, 2002] and fire spread rates [*Sedano and Randerson*, 2014] through their influence on convection, fire weather, and fuel moisture. The moisture content of fine surface fuels rapidly responds to variations in vapor pressure deficit over a period of hours or days, whereas the moisture content of deeper soil layers responds to the cumulative effects of precipitation and evapotranspiration over the course of the fire season [*Van Wagner*, 1987]. In permafrost areas, soil moisture is also regulated by heat inputs that influence thaw rates of the active layer [*Lawson*, 1986]. The likelihood of deep burning, high levels of fuel consumption, and enhanced carbon emissions are sensitive to the moisture levels of deeper layers [*Kasischke et al*., 1995; *Turetsky et al*., 2011; *Veraverbeke et al*., 2015].

Climate and weather variability influence the energy release during combustion and the depth of burning in organic soils [*Nash and Johnson*, 1996; *Turetsky et al*., 2011] and as such govern the amount and composition of trace gases emitted from fire. Flaming combustion is responsible for the more highly oxidized gas emissions such as CO_2, H_2O, NO_x, SO_2, and black carbon, whereas smoldering combustion produces most of the CO, CH_4, nonmethane volatile organic compounds, and primary organic aerosol [*Akagi et al*., 2011]. Smoldering and flaming combustion often occur simultaneously during a fire, and smoldering fires often exist as residual burning after a flaming fire front has moved through a particular area. Flaming combustion likely accounts for most of the fire spread under hot and dry conditions, whereas smoldering fires move more slowly, often in more humid conditions, but may contribute to combustion losses over longer intervals [*Akagi et al*., 2011; *Turetsky et al*., 2015]. Variables such as fuel moisture content and wind speed can influence the quantity of biomass consumed during either flaming or smoldering combustion phases [*Akagi et al*., 2011; *French et al*., 2014]. *Anderson et al.* [2015], for example, found that integrating fire weather conditions into a carbon emissions model increases the spatial and temporal variability of the emissions time series. Although the influence of weather on fire behavior and spread rate is well established in boreal ecosystems [*Alexander*, 1982; *Van Wagner*, 1987; *Abatzoglou and Kolden*, 2011; *Sedano and Randerson*, 2014], quantitative models linking weather with emissions and emission factors are currently lacking. In this context, new modeling approaches and atmospheric trace gas observations are needed to improve our understanding of how the composition of boreal fire emissions may respond to new extremes in fire weather.

Several approaches exist for estimating carbon emissions from fires. One paradigm is the *Seiler and Crutzen* [1980] approach whereby emissions are estimated as the product of area burned, fuel loads, the fraction of fuels combusted, and emission factors for different gas species that relate trace gas production to a fixed amount of consumed biomass. In boreal forests, this approach has been used extensively, along with advances in remote sensing, to estimate emissions [*French et al*., 2002; *Kasischke et al*., 2005]. *Veraverbeke et al.* [2015] estimated pyrogenic carbon consumption from relationships between field observations of carbon consumption and environmental variables, including a remotely sensed indicator of burn severity. They also leveraged the Moderate Resolution Imaging Spectroradiometer (MODIS) active fire/thermal anomaly data to obtain burned area and thus carbon emissions with a daily time step. Major sources of uncertainty with these modeling approaches include uncertainties in the algorithms used to estimate the amount of carbon consumed from aboveground and belowground carbon pools [*French et al*., 2004; *Veraverbeke et al*., 2015]. Errors for trace gases and aerosols are likely amplified by the use of temporally and spatially uniform emission factors.

Remote sensing also allows development of top down models of emissions from fires using an approach based on fire radiative energy. Previous studies have established a relationship between fire radiative energy and smoke aerosol or trace gas emission rates [*Wooster et al*., 2005; *van der Werf et al*., 2006; *Kaiser et al*., 2009]. The rate at which a fire releases energy has a direct, linear relationship to its rate of biomass consumption [*Ichoku and Kaufman*, 2005; *Wooster et al*., 2005]. Multiple satellite observations per day are needed to construct a diurnal cycle of fire radiative power (FRP), and the integral of this diurnal cycle, fire radiative energy, is directly related to total emissions. Remote sensing information on the number of thermal anomaly detections, such as active fire counts and FRP measurements from the MODIS sensors on the Terra and Aqua satellites, have been used to assign spatial and temporal variability in emissions. For example, *Wiedinmyer et al.* [2011] assigned a biome-specific burned area to MODIS active fire detections, enabling the creation of a global daily emissions time series at a 1 km resolution and in near real time. Similarly, *Mu et al.* [2011] used active fires from MODIS and Geostationary Operational Environmental Satellite radiometers to redistribute monthly fire emissions from the Global Fire Emissions Database to daily and 3-hourly resolutions.

Smoke modeling systems rely on the emissions models described above to simulate fire impacts on regional air quality [*Longo et al*., 2007; *Freitas et al*., 2009]. For this class of model, fire emissions estimates can be combined with an atmospheric transport model to estimate regional concentrations of aerosols or trace gases [e.g., *Grell et al*., 2011]. The BlueSky smoke modeling framework uses a modular assimilation of fire information, fuel loading, fuel consumption informed with meteorology, and aerosol emission factors to ultimately provide information about aerosol concentrations and the dispersion of fire plumes [*Larkin et al*., 2010]. Environment and Climate Change Canada's North American air quality forecast system, FireWork, uses near real time wildfire emissions estimates and a similar modeling framework that incorporates the BlueSky Fire Emissions Product Simulator module to provide regional forecasts of trace gases and aerosols [*Pavlovic et al*., 2016].

Here we examined the influence of daily meteorology on fire emissions and trace gas variability in interior Alaska as a part of NASA's Carbon in Arctic Reservoirs Vulnerability Experiment (CARVE). In a first step, we assessed the relative importance of different meteorological variables and fire weather indices in explaining the temporal variability of active fires, fire radiative power, burned area, and emissions within the state of Alaska during the summer of 2013. In a second step we combined estimates from the Alaskan Fire Emissions Database (AKFED) with an atmospheric model to simulate continuous trace gas observations from the CARVE-NOAA Global Monitoring Division tower in Fox, Alaska (hereafter referred to as the CRV tower) [*Karion et al*., 2016b]. We used the AKFED model because it was developed and constrained specifically for our region of study and because of its high spatial and temporal resolution. In our approach we use the coupled Polar Weather Research and Forecasting/Stochastic Time-Inverted Lagrangian Transport model (PWRF-STILT) to link emissions with trace gas observations at the CRV tower [*Henderson et al*., 2015]. This approach also allowed us to isolate contributions from individual fires to observed trace gas time series. To help constrain the transport model, we used CRV tower observations during high fire periods to estimate emission factors for carbon monoxide and methane and remote sensing observations to estimate plume injection heights.

2. Methods

2.1. Meteorological Data

We used daily meteorological summaries from the National Climatic Data Center (http://www7.ncdc.noaa.gov/CDO/cdopoemain.cmd) for three stations in interior Alaska to assess synoptic-scale variability in fire weather. These stations were the Fairbanks International Airport, Eielson Air Force Base, and Minchumina. The Fairbanks and Eielson stations were selected because of their close proximity to the Stuart Creek II and Mississippi fires that accounted for about 12% of the total burned area in interior Alaska during 2013. Minchumina was selected because of its proximity to a set of fires to the southwest of Fairbanks, near Denali National Park (Figure 1). At each station we extracted hourly precipitation, mean surface air temperature, dew point temperature, and wind speed. Hourly relative humidity for each station was calculated using the August-Roche-Magnus approximation with the dew point and air temperature time series [*Lawrence*, 2005]. Hourly saturation vapor pressure was calculated following *Tetens* [1930] as a nonlinear function of temperature. Hourly vapor pressure deficit (VPD) was calculated by subtracting the actual vapor pressure from the saturation vapor pressure. We extracted the noon local time data for precipitation, temperature, relative humidity, and wind speed to compare with the fire weather indices described below.

We used the noon local standard time observations described above to estimate fire indices from the Canadian Forest Fire Weather Index System [*Van Wagner*, 1987]. This system has three codes to characterize the moisture of fuel classes. The fine fuel moisture code (FFMC) is representative of fine fuels such as litter consisting of a dry weight layer approximately 1.2 cm deep. The FFMC attempts to capture the relatively fast drying of fine fuel in response to temperature, relative humidity, wind speed, and rainfall on short timescales. It has been used to indicate ease of ignition or ignition probability [*Van Wagner*, 1987]. The duff moisture code (DMC) provides a metric for loosely packed decomposing organic material in surface soils 7 cm deep. The drought code (DC) represents deep compact organic material 18 cm deep and is an indicator of potential depth of burn. Each of these codes depends on a combination of temperature, humidity, wind speed, and precipitation. Three additional indices are derived from these codes. The initial spread index (ISI) combines wind and the FFMC to estimate fire weather influence on the spread rate. The buildup index (BUI) combines the duff moisture code and the drought code. The fire weather index (FWI) combines ISI and BUI to represent

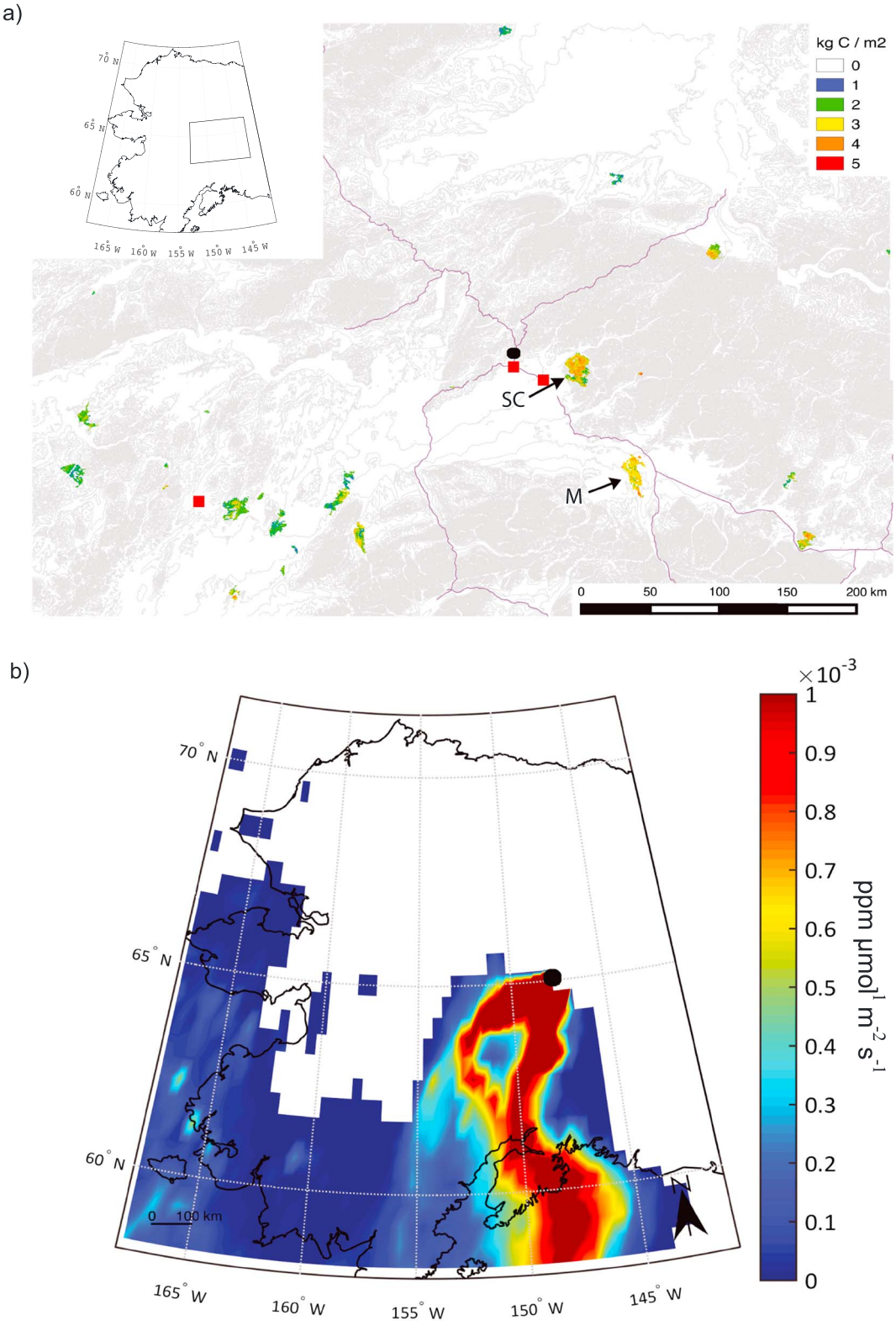

Figure 1. (a) Map of fire characteristics in our Alaska study domain during the summer of 2013. Alaska Fire Emissions Database (AKFED) total carbon emissions from fires are shown in kg C per m^2. (b) The daily mean of all PWRF-STILT footprints during a representative high fire period on 5 July 2013. In both panels, the location of CRV tower is denoted with a black circle, and Figure 1a the location of the Minchumina, Fairbanks International Airport, and Eielson Air Force Base weather stations are shown from left to right with red squares. In Figure 1a, the locations of the Stuart Creek II fire and the Mississippi fire are denoted by SC and M, respectively, major roads are shown as purple lines, and elevation is shown with gray shading.

the energy release by the fire per unit length of fire front. In our analysis, we examined the ability of these indices from the Canadian Forest Fire Weather Index System that are aimed at capturing variability in fire spread rates. The FFMC, ISI, and FWI indices are widely used by the fire management community to quantify different aspects of fire behavior and risk.

2.2. Emission Factors

We used high-resolution measurements from the CRV tower [*Karion et al*., 2016b] during periods of high fire influence from the summer of 2013 to determine emission factors for our modeling analysis. A CO threshold of 0.7 ppm was applied to isolate periods when fires had significant influence on CO_2 mole fraction. We estimated emission ratios by calculating the slope of CRV tower CO and CH_4 enhancements above background (ΔCO and ΔCH_4) relative to that of CO_2 (ΔCO_2). The Δ refers to CRV tower observations of trace gas mole fractions with background values subtracted. We applied a type II linear regression and then multiplied by a scalar to convert the molar ratio into grams of species emitted per kilogram of biomass burned, assuming 450 g C are emitted per kilogram of biomass burned [*Yokelson et al*., 1997; *Akagi et al*., 2011]. We used estimates from *Karion et al.* [2016a] to remove background levels of CO, CH_4, and CO_2. For CO_2 we also estimated and removed the influence of net ecosystem exchange (NEE) associated with gross primary production and ecosystem respiration fluxes. CO_2 anomalies originating from NEE were estimated by coupling the Polar Vegetation Photosynthesis Respiration Model (PVPRM) [*Luus and Lin*, 2015] fluxes with PWRF-STILT [*Henderson et al*., 2015] simulations at the CRV tower. PVPRM provided 3-hourly estimates of net ecosystem exchange from high-latitude ecosystems for regions north of 55°N.

2.3. Plume Heights From the Multiangle Imaging Spectroradiometer (MISR)

The PWRF-STILT model used to quantify the influence of terrestrial net ecosystem exchange on CO_2 variability at CRV assumes that upwind air parcels that are transported within the bottom half of the planetary boundary layer are subsequently modified by surface exchange. Fire emissions, in contrast, have the potential to be injected in fast rising plumes through the full boundary layer and into the free troposphere [*Duck et al*., 2007; *Leung et al*., 2007; *Turquety et al*., 2007; *Kahn et al*., 2008]. Here we directly measured fire plume heights to create a better representation of fire injection in PWRF-STILT. The MISR instrument on Terra provides stereographic images of clouds and plumes, enabling the retrieval of height information [*Kahn et al*., 2008]. We used the MISR Interactive Explorer (MINX) software program [*Nelson et al*., 2013] to manually digitize the plume perimeters from all available imagery in Alaska during the summer of 2013. Plume heights were then computed by MINX for each 1 km MISR pixel in each perimeter, along with aggregate statistics of the mean, standard deviation, and maximum heights. In parallel we extracted boundary layer heights at the time of the MISR overpass from Modern-Era Retrospective Analysis for Research and Applications (MERRA) [*Reichle et al*., 2011]. As described below in section 3.3, we found the mean plume heights were approximately the same as the boundary layer heights. Thus, results below defined the surface influence volume in STILT as extending from the surface to the top of the planetary boundary layer (PBL), with the assumption that the fire emissions were equally distributed within the PBL [*Turquety et al*., 2007; *Kahn et al*., 2008].

2.4. Active Fires, Fire Radiative Power, and the 2013 Fire Season

The spatial and temporal variability of active fires and fire radiative power was determined using fire detection observations from MODIS on NASA's Terra and Aqua satellites [*Giglio et al*., 2003]. We specifically used the MCD14ML product and report fire detections for all confidence levels, because commission errors are generally low in boreal forest ecosystems. Observations between 58° to 71.5°N and 141° to 168.5°W were aggregated to create a daily time series with a 0.5° spatial resolution.

The 2013 Alaskan fire season had levels of fire activity, burned area, and emissions that were somewhat below long-term means. Annual burned area from AKFED in 2013, for example, was 533 kha compared with a 2001–2010 mean of 655 kha/yr. Similarly, carbon emissions were 12.7 Tg C compared with a decadal average of 18 Tg C per year [*Veraverbeke et al*., 2015]. In this context, it is also important to note that the year-to-year variability of wildfire emissions is extremely high in Alaskan forests. During 2001–2010 emissions were at a maximum in 2004 at 69 Tg C and were at a minimum in 2008 at 1 Tg C.

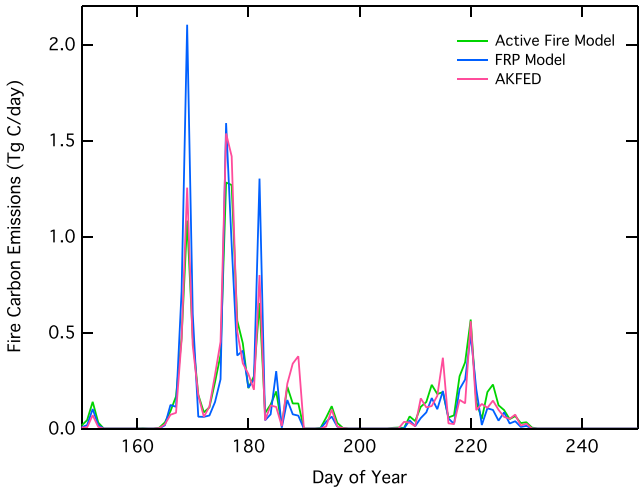

Figure 2. Time series of total daily fire carbon emissions (Tg C/d) for the active fire, fire radiative power (FRP), and Alaska Fire Emissions Database (AKFED) modeling approaches.

2.5. Emissions Modeling

We compared the ability of three different fire emissions modeling approaches to capture variability in trace gas observations measured at the CRV tower. The three approaches were derived from satellite-derived observations of active fires, satellite-derived estimates of FRP, and daily emissions estimates from AKFED [*Veraverbeke et al.*, 2015]. Each approach provided a slightly different temporal and spatial distribution of emissions in interior Alaska. AKFED is an empirical model of carbon consumption with a spatial resolution of 450 m and a temporal resolution of 1 day. Measurements of prefire fractional tree cover, difference normalized burned area, elevation, and day of burning determines fuel consumption in aboveground vegetation and soil organic layers. The timing of carbon releases in AKFED is determined by assigning the timing of the closest active fire detection for each burned pixel. The AKFED model estimated an annual total of 12.7 Tg C of emissions within our study domain during 2013 (Figure 1).

For the active fire emissions model, MODIS Aqua and Terra observations of active fires were binned each day to the resolution of our atmospheric model (0.5°). We then applied a conversion scalar (S_{FC}) to convert active fires into kg of carbon. S_{FC} was derived as the ratio of the annual sum of total emissions from AKFED and the annual sum of active fires within our domain. With this approach, the annual sum was constrained to yield the same annual integral of emissions; however, the spatial and temporal pattern of emissions was determined solely by the spatial distribution and timing of active fires.

$$E_{FC}(x,t) = \frac{S_{FC} \times FC\ (x,t)}{A\ (x)} \tag{1}$$

where E_{FC} is the fire emissions with units of kg C m^{-2} d^{-1} in grid cell x and at day t, S_{FC} is the globally uniform scalar with units of kg C per active fire detection, FC is the sum of active fire detections in the grid cell each day, and A is the land surface area of each grid cell. The FRP model had a similar form:

$$E_{FRP}\ (x,t) = \frac{S_{FRP} \times FRP\ (x,t)}{A\ (x)} \tag{2}$$

where E_{FRP} is the fire emissions with units of kg C m^{-2} d^{-1}, S_{FRP} is the globally uniform scalar with units of kg C per MW, and FRP is the sum of fire radiative power for all of the active fires in the grid cell each day. AKFED provides an output of daily fire emissions with units of kg C m^{-2} d^{-1}, and these emissions were averaged within each 0.5° grid cell of the atmospheric model. The daily time series of the AKFED, active fire, and FRP-derived emissions derived using these approaches are shown in Figure 2.

2.6. CRV Tower Observations

Atmospheric CO, CH_4, and CO_2 mole fractions during the summer of 2013 were measured at the CRV tower in Fox, Alaska (Figure 1a) using a cavity ring-down spectrometer (CRDS, Picarro models 2401 and 2401 m) [*Karion et al.*, 2016a, 2016b]. The tower is 32 m in height and is located on a ridge 611 m above sea level in central Alaska at 64.986°N, 147.598°W. Atmospheric measurements from air drawn from 5 m, 17 m, and 32 m heights from the base of the tower are averaged in 30 s increments (native measurement frequency for these CRDS units is approximately 0.5 Hz). In this study we used observations only from the 32 m intake because this level had the highest measurement density, with observations for 50 min out of every hour,

and because this level was likely to have the smallest sensitivity to local ecosystem fluxes near the tower [*Karion et al*., 2016a].

The raw 30 s average measurements were processed by applying a water correction that was empirically determined in the laboratory prior to deployment of each CRDS unit, following procedures similar to those described in previous studies [*Chen et al*., 2013; *Rella et al*., 2013]. The CRDS instruments were calibrated using five reference tanks with mole fractions traceable to the WMO standard scales for all three gases, and drift-corrected using the average drift of two tanks (also traceable to WMO standard scales) were measured every 8 h. Total uncertainty (reproducibility and comparability to other NOAA network sites) of hourly mole fraction measurements at the site are generally $<$0.2 ppm for CO_2, 2 ppb for CH_4, and 5 ppb for CO (1 sigma). The measurement system at the CRV tower is described in more detail by *Karion et al.* [2016b].

2.7. Atmospheric Modeling

STILT [*Lin et al*., 2007] is a Lagrangian Particle Dispersion Model, coupled offline to the PWRF regional atmospheric numerical weather prediction model [*Skamarock et al*., 2005; *Chang et al*., 2014; *Henderson et al*., 2015], that computes the sensitivity—effectively the adjoint of the transport model—of measured atmospheric trace gas measurements to upwind fluxes in the form of a surface influence function (the "footprint" field; units of mole fraction/(μmol m^{-2} s^{-1})). We note that the spatial resolution of the PWRF model is 3.3 km over interior Alaska; however, the PWRF-STILT footprints were evaluated on a 0.5° $\times$ 0.5° aggregated grid [e.g., *Chang et al*., 2014; *Henderson et al*., 2015]. Each footprint field is calculated by counting the number of particles released in a reverse-time simulation in a surface-influenced volume and the time spent in that volume [*Lin et al*., 2007]. In this study, 500 particles were released from the receptor location at each time step for the footprint calculations. To obtain the contribution (units of mole fraction) by the upwind fluxes to the observed concentration, the footprint field is convolved with an estimate of the upwind fluxes. *Nehrkorn et al.* [2013], for instance, studied the transport of CO_2 in Salt Lake City using WRF-STILT footprints in which the depth of the atmospheric layer influenced by surface fluxes was defined as half the depth of the PBL.

We used PWRF-STILT footprints to determine the contribution of fire emissions to CO, CH_4, and CO_2 mole fraction observations at the CRV tower. The footprints for CRV are on a 0.5° latitude-longitude grid with a temporal resolution of 1 h during the day (hours 0600 to 1800 local time) and 3 h during the night (hours 1800 to 0600). An example of the spatial distribution for the daily mean of footprints for the study period is shown in Figure 1b. The footprints are multiplied by an a priori flux field, defined here as the fire emissions (E_{FC}, E_{FRP}), to quantify the mole fraction measured at the CRV tower location. To identify sensitivities to the injection height, the definition of the top of the surface-influenced layer in STILT was varied from the default of half the depth of the PBL to, respectively, 1.0 and 1.5 times the depth of the PBL. For each case, the flux remained the same, but the vertical resolution of the surface-influenced volume was modified. For the 1.0 PBL case, which best matched the MISR plume observations, the influence of fire emissions on CRV trace gas mole fractions was reduced by approximately 14% relative to the model default. All other aspects of the modeling system follow directly from *Henderson et al.* [2015].

To impose diurnal variation in the fire emissions, we binned daytime (0600 to 1800) and nighttime (1800–0600) FRP each day in each grid cell and assumed the relative fractions of FRP were proportional to emissions. Emission factors (g trace gas species (kg biomass)$^{-1}$) were used to convert total carbon emissions to CO, CH_4, and CO_2 emissions. We obtained and implemented emission factors from the CRV tower measurements as described below.

3. Results

3.1. Influence of Variability in Daily Meteorology on Fire Activity and Emissions

Two distinct high fire periods occurred during the summer of 2013 in interior Alaska, as measured using the number of satellite-detected active fires (Figure 3a). The first, between day of year (DOY) 168 and 192, was coincident with the highest midday surface air temperatures (Figure 3b) and lowest relative humidity levels of the year (Figure 3c). Precipitation during this interval was low, with only a single significant event recorded at Fairbanks Airport and Minchumina on DOY 173 and several smaller precipitation days observed between DOY 180 and 185 (Figure 3d). A second period of fire activity occurred between DOY 210 and 230. High temperatures, low relative humidity, and an absence of precipitation events also characterized this second

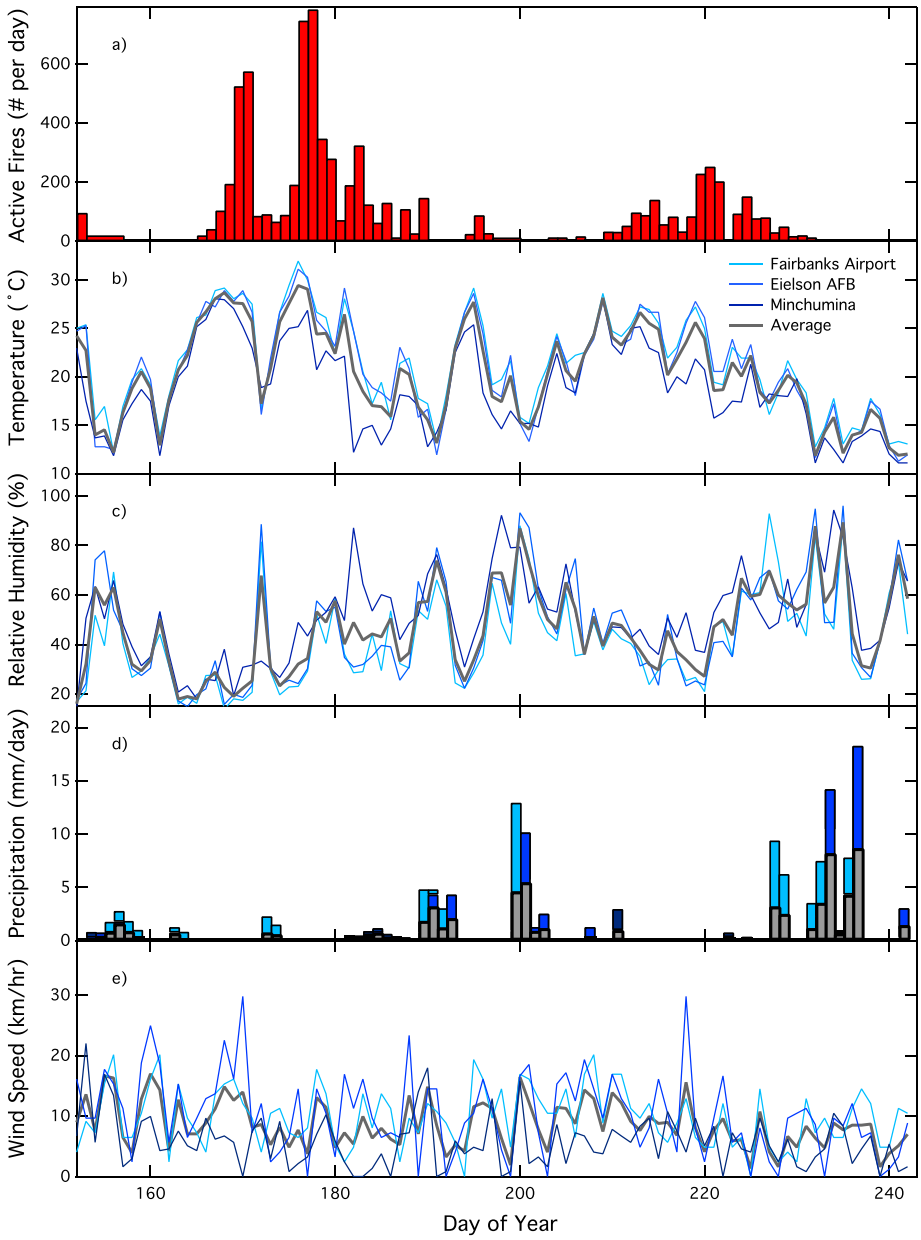

Figure 3. Comparison of daily weather variables from three stations in interior Alaska, including Fairbanks International Airport, Eielson Air Force Base, and Minchumina. The different panels show (a) the number of active fires per day, (b) temperature (C°), (c) relative humidity (%), (d) precipitation (mm/d), and (e) wind speed (km/h). All of the variables except precipitation represent the hourly average at noon local standard time. Precipitation is the 24 h sum.

period. Wind speeds were variable throughout the season (Figure 3e). After DOY 230, a series of precipitation events terminated the 2013 fire season.

To assess the influence of daily meteorology in modulating regional fire activity, burned area, and emissions, we conducted a regression analysis with individual daily meteorological variables and fire weather indices. Among the different variables shown in Figure 3, daily temperature was most strongly correlated with the different fire products, followed by relative humidity, precipitation, and wind speed (Table 1). VPD, derived from a combination of temperature and relative humidity, was slightly better than temperature as a predictor for FRP and burned area but had about the same level of performance for the other fire time series. The relatively high performance of VPD as a predictor for burned area observed here is consistent with earlier work

Table 1. Pearson's Coefficient of Determination (r^2) Between Daily Weather Variables, Fire Weather Indices, and Time Series Fire Activity[a]

	Meteorological Variables					Fire Weather Indices					
	T	RH	*P*	WS	VPD	FFMC	DMC	DC	ISI	BUI	FWI
Active fires	0.32	0.11	0.05	0.000	0.31	0.20	0.17	0.02	0.18	0.09	0.28
Fire radiative power (FRP)	0.20	0.09	0.03	0.001	0.23	0.15	0.11	0.03	0.18	0.04	0.24
AKFED burned area	0.28	0.12	0.04	0.000	0.31	0.21	0.15	0.04	0.21	0.06	0.29
AKFED emissions	0.25	0.09	0.04	0.001	0.25	0.17	0.18	0.03	0.14	0.08	0.23

[a]All correlations were significant at $p < 0.05$ except for precipitation and the drought code. These daily correlations were computed over the period from day of year 152 to day of year 242. The weather variables we analyzed included temperature (*T*), relative humidity (RH), precipitation (*P*), wind speed (WS), and vapor pressure deficit (VPD). The fire weather indices included the fine fuel moisture code (FFMC), duff moisture code (DMC), drought code (DC), initial spread index (ISI), buildup index (BUI), and fire weather index (FWI). The Alaskan Fire Emissions Database is abbreviated as AKFED.

indicating that VPD anomalies in interior Alaska synchronizes spread rates across multiple fires [*Sedano and Randerson*, 2014].

Of the six fire weather indices that we analyzed from the Canadian Forest Fire Weather Index System, FFMC, ISI, and FWI indices had the strongest relationships with the daily time series of fire activity. The FFMC and ISI indices were moderately correlated with daily fire activity, explaining between 14 and 21% of the variance of the different daily fire time series (Table 1 and Figure 4). FWI was the most successful predictor of all of the different fire weather indices examined here, capturing between 24% of the variance for FRP and 29% for burned area. Compared with the meteorological variables, FWI had a similar level of predictive capacity as VPD and temperature.

3.2. Emission Factors

We identified six periods of significant fire influence when a synchronized enhancement of CO, CH_4, and CO_2 was observed at CRV tower during July and August. We used these intervals to estimate emission factors for CO and CH_4 (Figure 5). Emission factors for CO ranged from 104 to 166 g CO per kg of combusted biomass and emission factors for methane varied between 6.26 and 8.96 g CH_4 per kilogram of combusted biomass (Table 2 and Figure 6). All six periods had high correlations between ΔCO and ΔCO_2 (r between 0.96 and 0.99) and between ΔCH_4 and ΔCO_2 (*r* values ranging between 0.96 and 0.99). Averaging across these periods, the mean $\Delta CO/\Delta CO_2$ emission factor was 134 ± 25 g CO per kg of combusted biomass and the mean $\Delta CH_4/\Delta CO_2$ emission factor was 7.74 ± 1.06 g CH_4 per kilogram of combusted biomass. The errors associated with the final average emission factors were calculated as one standard deviation between the average emission factors for all six of the high fire periods. We used these mean emission factors in our transport model simulations of fire contributions to the CRV tower described below sections 3.4.

3.3. Injection Heights

We digitized a total of 35 individual fire plumes in our study domain during the summer of 2013 to extract injection heights from the MISR imagery. This set represented all of the fire plumes we could visibly identify from the complete set of available MISR imagery, aided by MODIS active fire detections, between DOY 130 and DOY 270. The plumes had an average mean height and standard deviation of 1250 ± 551 m above terrain and an average maximum height of 2480 ± 931 m above terrain (Figure 7). We separated the plume and boundary height information into two periods corresponding to the first and second high fire periods visible in Figure 3a. The first covered the interval from DOY 168 to 192 and the second from DOY 210 to 230. Maximum plume heights during the first high fire period were significantly higher ($p < 0.02$) than during the second period (2920 ± 636 versus 2300 ± 980 m above terrain). Mean plume heights, however, were not significantly different between the two periods.

Planetary boundary layer height estimates from Modern-Era Retrospective Analysis for Research and Applications (MERRA) reanalysis, sampled on the same days and grid cells as the plume observations, had a mean of 1520 ± 450 m. For 20 out of the 35 plume observations, the MERRA planetary boundary layer was higher than the mean but lower than the maximum reported plume heights from MISR. Considering

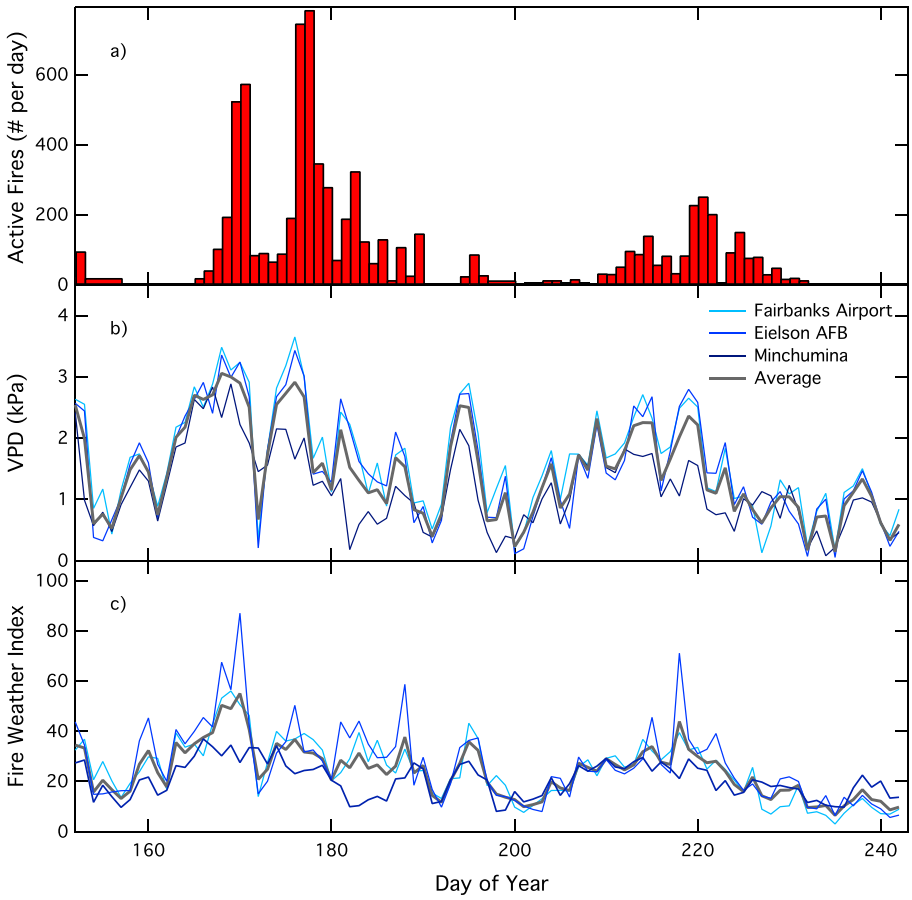

Figure 4. Comparison of daily complex weather variables from Fairbanks Airport, Eielson Air Force Base, Minchumina, and the average. (a) The number of active fires per day. (b) Vapor pressure deficit (VPD). (c) The Canadian Forest Fire Weather Index (FWI).

the relatively high level of agreement between planetary boundary layer and plume heights, and moderate levels of uncertainty in estimating both of these measures, we modified PWRF-STILT for the fire simulations so that the surface-influenced volume extended through the full planetary boundary layer height in each grid cell (see section 2.7).

3.4. Modeling Fire Contributions to Trace Gas Variability

During the summer of 2013 there were two periods during which elevated CO and CH_4 were observed at the CRV tower (Figure 8). The first period occurred from DOY 186 to 189, and the second period occurred from DOY 221 to 222. During the first period in July maximum trace gas mole fractions were 6.91 ppm for CO, 2.15 ppm for CH_4, and 411 ppm for CO_2. Similarly, during the second period in August maximum observed mole fractions were 2.57 ppm CO, 2.14 ppm CH_4, and 412 ppm CO_2. As described below, the synchronized enhancement of all three trace gas species during these two time periods indicated that fire emissions were a driver of the observed variability.

The model simulations combining fire emissions with PWRF-STILT provided evidence that the two anomalously high periods of CO and CH_4 at the CRV tower were attributable to boreal fire emissions from interior Alaska (Figure 8). For AKFED, the model had a correlation coefficient of 0.68 with observed daily mean CO and had a high bias of approximately 60%. CO estimates from the model driven by active fires or FRP had similar levels of correlation with the observations as AKFED (Table 3), although the timing of individual daily peaks varied among the different emissions sources (Figure 8a). These results suggest the performance of AKFED, in terms of capturing daily and synoptic variability in trace gas variability, was similar to more

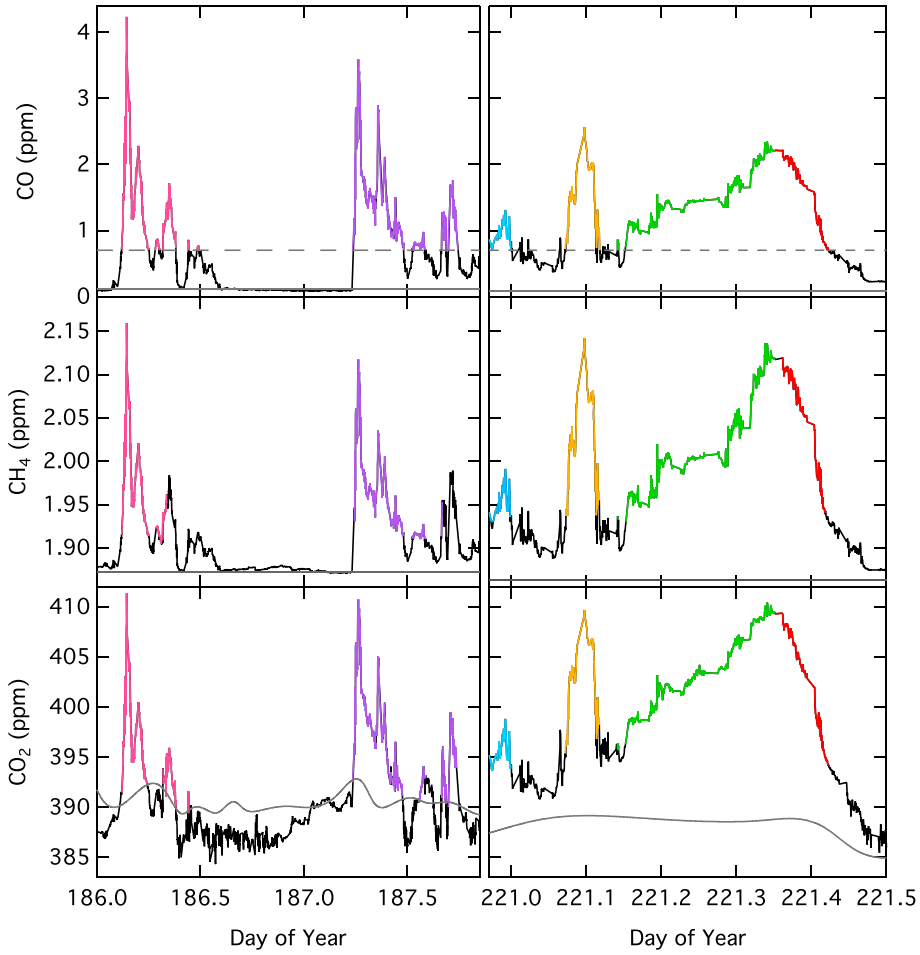

Figure 5. The original data from the CRV tower used to calculate emission ratios. (left column) July and (right column) August. (top row) CO (ppm), (middle row) CH_4 (ppm), and (bottom) CO_2 (ppm) are displayed. Background threshold for CO is given by dashed gray line; backgrounds for CH_4 and CO_2 are shown by solid gray lines. The time intervals used in emission ratio calculations are highlighted in color: July period 1 (pink), July period 2 (purple), August period 1 (blue), August period 2 (orange), August period 3 (green), and August period 4 (red).

established approaches that have relied on active fires to capture fine temporal scale variability in emissions [e.g., *Mu et al.*, 2011]. Our model simulations were able to explain a smaller amount of the variability in CH_4 (Figure 8b), which is consistent with the response of widespread methane sources in lowland ecosystems of interior Alaska responding in parallel to the synoptic-scale variability shown in Figure 3 [*Chang et al.*, 2014]. Fires explained only a very small amount of the variability in atmospheric CO_2 during the growing season period (Figure 8c). This finding is consistent with only moderate levels of fire emissions observed during 2013 in Alaska (12.7 Tg C) that were slightly below the decadal annual mean (18 Tg C/y) [*Veraverbeke et al.*, 2015] and a dominant role of photosynthesis and ecosystem respiration in influencing surface atmospheric CO_2 variability on synoptic and seasonal timescales in high-latitude ecosystems [*Luus and Lin*, 2015; *Karion et al.*, 2016a].

3.5. Individual Fire Contributions to Modeled Trace Gas Mole Fractions

The combined AKFED-PWRF-STILT model allowed us to isolate the daily contribution of individual fires to simulated trace gas simulations at the CRV tower. In our analysis, we separated contributions from the Stuart Creek II fire, which was located approximately 58 km southeast of the tower, and the Mississippi fire, which was located about 144 km southeast of the tower, from all other fires in the state. We identified the grid cells containing the individual fires of interest using burn perimeters from the Alaska Large Fire Database. We then masked all fire emissions in these grid cells to zero in AKFED and then reran the convolution of AKFED and PWRF-STILT. The individual fire contributions were then calculated by subtracting this

Table 2. Emission Ratios and Emission Factors (g Species Emitted per kg combusted biomass) From Selected Observations During High Fire Periods at CRV Tower[a]

				$\Delta CO/\Delta CO_2$		$\Delta CH_4/\Delta CO_2$	
Date	Time	Number of Data Points	Correlation CO (CH_4)	Emission Ratio	Emission Factor[b]	Emission Ratio	Emission Factor
July 5—P1	12 A.M. to 12 P.M.	183	0.98 (0.98)	0.158 ± 0.002	166 ± 2.1	0.0110 ± 0.0002	6.62 ± 0.12
July 6—P2	5 A.M. to 7 P.M.	325	0.97 (0.96)	0.152 ± 0.002	160 ± 2.1	0.0104 ± 0.0002	6.26 ± 0.12
August8—P1	10:30 P.M. to 12 A.M.	74	0.96 (0.96)	0.122 ± 0.004	128 ± 4.2	0.0137 ± 0.0005	8.24 ± 0.30
August 9—P2	1:30 A.M. to 3 A.M.	96	0.99 (0.99)	0.127 ± 0.002	133 ± 2.1	0.0149 ± 0.0002	8.96 ± 0.12
August 9—P3	3:30 A.M. to 8:30 A.M.	443	0.97 (0.97)	0.099 ± 0.0002	104 ± 0.2	0.0136 ± 0.0002	8.18 ± 0.12
August 9—P4	8:30 A.M. to 10:30 A.M.	139	0.99 (0.99)	0.109 ± 0.0008	114 ± 0.8	0.0136 ± 0.0001	8.18 ± 0.06
Mean				0.128 ± 0.023	134 ± 25	0.0139 ± 0.0018	7.74 ± 1.06

[a]Correlations are given as Pearson's correlation coefficient (*r*).
[b]To estimate emission factors from emission ratios, we assumed that combusted biomass was comprised of 45% carbon [*Yokelson et al.*, 1997; *Akagi et al.*, 2011].

version of the combined AKFED-PWRF-STILT model from the original simulation. The Stuart Creek II fire accounted for 75% of the total CO mole fraction signal from fire when integrated over the fire season, whereas the Mississippi fire accounted for 6% of the signal at the CRV tower—with most of its impact occurring during the second high fire period (Figure 9). Other more remote fires were responsible for the remaining 19% of the CO mole fractions at the CRV tower. The capability to link individual fires to tower observations is novel and may allow the exploration of relationships between regionally varying ecosystem processes and trace gas emissions and composition in future work.

4. Discussion

4.1. The Influence of Daily Variations in Meteorology on Fire Activity

Daily variability in meteorology is well known to influence many aspects of boreal fire behavior [*Johnson*, 1996]. Here we found that temperature and vapor pressure deficit were the most important meteorological fields to explain daily fire activity during the summer of 2013. The importance of these variables has been noted in past studies at different temporal and spatial scales [*Flannigan and Harrington*, 1988; *Bessie and Johnson*, 1995; *Duffy et al.*, 2005; *Sedano and Randerson*, 2014]. Monthly burned area in different Canadian provinces was shown to vary considerably as a function of extended periods of days with low precipitation or relative humidity [*Flannigan and Harrington*, 1988]. *Duffy et al.* [2005] found that June temperature was an important variable in explaining year-to-year variations in Alaskan burned area. VPD is an indicator of fire spread in boreal forest ecosystems, and the sum of positive daily VPD anomalies is correlated with annual burned area [*Sedano and Randerson*, 2014].

The Canadian Forest Fire Weather Index System has been used extensively to quantify past, present, and future patterns in fire behavior [*Stocks et al.*, 1998; *Flannigan et al.*, 2001; *Bergeron et al.*, 2004; *Bedia et al.*, 2015]. For example, *Stocks et al.* [1998] found that under a doubled CO_2 scenario, the fire season started earlier and areas with high to extreme fire danger expanded across Canada and Russia. *Bedia et al.* [2015] found that fire weather in boreal forests will become increasingly sensitive to short-term climate fluctuations in a warming scenario to 2045. We found that temperature and VPD had a similar level of predictive capacity as FWI and that FWI performed better than all of the other fire weather indices. Although the Canadian Forest Fire Weather Index System is a useful tool for estimating future fire weather conditions, our results suggest other more direct weather variables, like VPD, also have the potential to explain variations in fire dynamics in boreal forest ecosystems. VPD has been used as a driver of a global scale prognostic fire model [*Pechony and Shindell*, 2009], and our results confirm that there is a strong mechanistic relationship between this variable and daily burned area and emissions in boreal North America.

4.2. CO and CH_4 Emission Factors

Although recent aircraft and ground observations have reduced uncertainties in wildfire emission factors for individual biomes [*Akagi et al.*, 2011], a lack of long-term time series of atmospheric composition data near large fire complexes limits our ability to dynamically model emission factors as a function of changing environmental conditions. For the boreal forest, relatively few direct measurements of emission factors exist, and

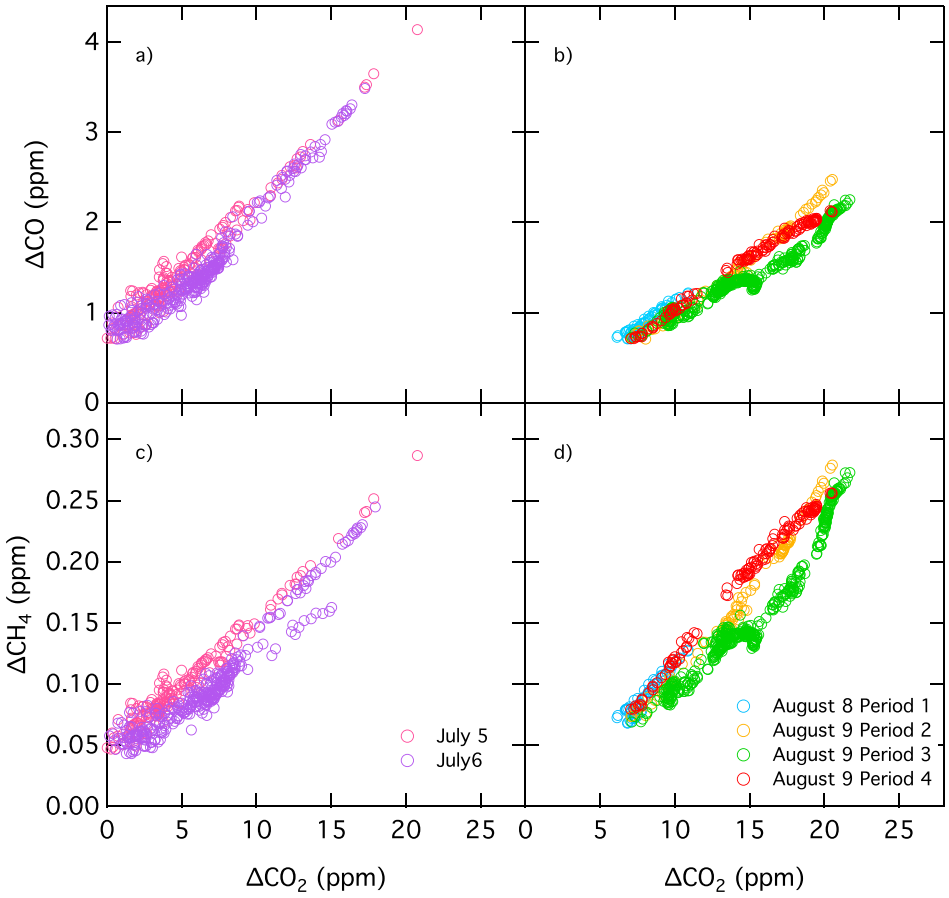

Figure 6. Relationship between ΔCO (CO observed - CO background) and ΔCO_2 (CO_2 observed - CO_2 background) for periods of high fire influence at the CRV tower in (a) July and (b) August. (c and d) Relationship between ΔCH_4 (CH_4 observed - CH_4 background) and ΔCO_2 (CO_2 observed - CO_2 background) is shown for the same two periods, respectively.

this has led to the prescription of biome-invariant values in large-scale fire models, like the Global Fire Emissions Database [*van der Werf et al.*, 2010], the Fire Inventory from the National Center for Atmospheric Research [*Wiedinmyer et al.*, 2011], and the Wildland Fire Emissions Information System [*French et al.*, 2014]. Previous aircraft and field campaigns have led to the sampling of 23 fresh boreal fire plumes over the last three decades using continuous flow gas analyzers [*Radke et al.*, 1991; *Nance et al.*, 1993; *Cofer et al.*, 1998; *Goode et al.*, 2000] and flasks [*Simpson et al.*, 2011]. A synthesis of these data by *Akagi et al.* [2011] yielded a mean CO emission factor of 127 ± 45 g CO per kg combusted biomass and a mean CH_4 emission factor of 5.96 ± 3.14 g CH_4 per kg combusted biomass. Here during two high fire periods, we obtained emission factors that were slightly higher than the mean from *Akagi et al.* [2011]. Our estimates of 134 ± 25 g CO per kg combusted biomass and 7.74 ± 1.06 g CH_4 per kg combusted biomass suggests that the 2013 Alaskan fires may have had a somewhat larger relative contribution from a smoldering combustion phase.

Our analysis suggests that continuous, high temporal resolution tower measurements of greenhouse gases in a high fire region can provide new information on emission factors that complements aircraft plume sampling. Even during a moderate fire season, we were able to identify six periods in which trace gas signals from individual fires were large enough to derive emission factors. While background CO and CH_4 concentrations were relatively constant over time, enabling a relatively clean separation of the anomaly caused by fires, CO_2 was much more variable due to numerous ecosystem sources and sinks that fluctuated on diurnal, synoptic, and seasonal timescales. This variability makes it critical to accurately simulate and remove the CO_2 variability originating from terrestrial net ecosystem exchange using ecosystem models and observations from low fire periods [*Karion et al.*, 2016a].

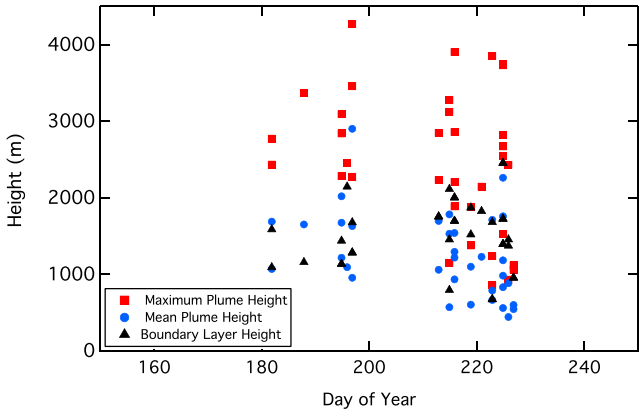

Figure 7. Daily Multiangle Imaging SpectroRadiometer (MISR) derived maximum plume heights (red squares) and mean plume heights (blue circles) compared with geographically and temporally matched Modern-Era Retrospective Analysis for Research and Applications (MERRA) boundary layer heights (black triangles).

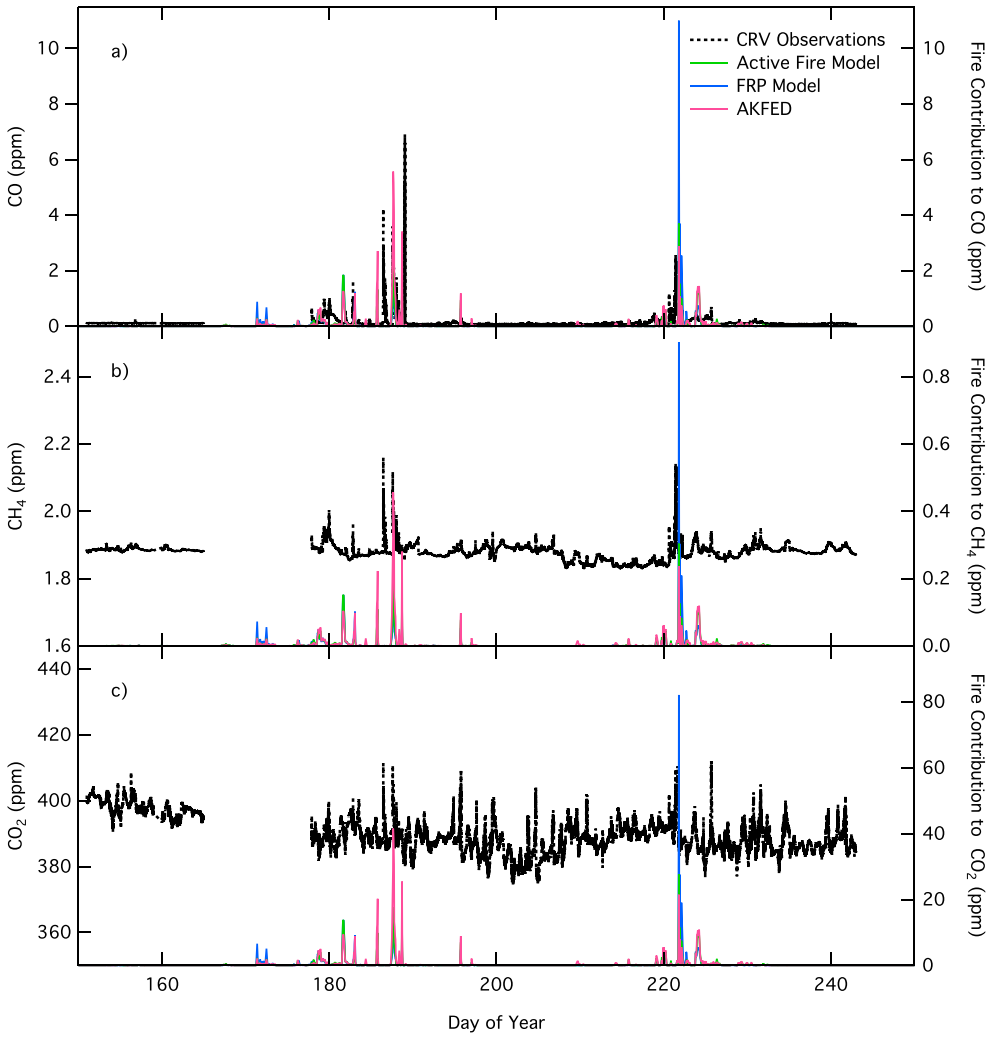

Figure 8. Observations from the CRV tower (black dashed line) versus active fire approach (green), FRP approach (blue), and AKFED (pink) for (a) CO (ppm), (b) CH_4 (ppm), and (c) CO_2 (ppm). Left *y* axis corresponds to CRV tower observations.

Table 3. Pearson's Correlation Coefficient (*r*) Between Daily Fire Emissions and Observations From CRV Tower[a]

	Active Fire Model	FRP Model	AKFED
CO hourly	0.65*	0.63*	0.68*
CH_4 hourly	0.45*	0.51*	0.42*
CO_2 hourly	0.10	0.18	0.04

*Significant correlations with *p* values <0.01. These correlations were computed using daily data over the period from DOY 152 to DOY 242.
[a]Background concentrations for CO, CH_4, and CO_2 were subtracted from CRV observations for this comparison.

Further work using high temporal resolution tower observations is necessary to understand environmental controls on boreal forest fire emission ratios. More observations may provide a way to relate emission factors to fire type (smoldering versus flaming), weather variability, land and tree cover, drainage status, soil moisture, and burn severity. The modeling approach developed here is well suited for studying these relationships because it allows for the identification of trace gas contributions from individual fires. More specifically, the use of PWRF-STILT in future work may make it possible to link environmental and weather variables at the time and location of a single wildfire to greenhouse gas mole fraction anomalies observed at a tower. The number of days with strong fire signals was relatively low during the summer of 2013, limiting our ability to investigate these relationships. An important next step in this context is to extend this analysis to the high fire seasons observed in the Canadian Northwest Territories in 2014 and in Alaska in 2015.

4.3. Top Down Constraints on Fire Emissions Inventories

In past studies, active fires and FRP have been widely used to distribute fire emissions in space and time [*Ichoku and Kaufman*, 2005; *Wooster et al*., 2005; *van der Werf et al*., 2006; *Jordan et al*., 2008; *Kaiser et al*., 2009], and in this study we show that AKFED had a similar performance to these more commonly used methods. The relationship between observed trace gas at the CRV tower and AKFED convolved with PWRF-STILT, with a correlation coefficient of 0.68, provides partial validation for AKFED. The difference and similarities among approaches are evident when the models are convolved with PWRF-STILT to predict carbon concentrations at CRV tower (Figure 8 and Table 3). All three approaches captured some of the fine-scale temporal dynamics of the fire signals as observed at the tower; however, on average, the signals were somewhat overestimated. Averaged over the fire season, AKFED had a positive bias of 60%. AKFED exhibits this bias primarily during the first fire period, whereas for the FRP-based model, the overestimation appears mostly during the second fire period. The three conceptual approaches show discrete differences in fire emissions both temporally (Figure 2) and spatially (Figure 1). Although conceptually distinct, the models are not completely independent, which contributed to their fairly similar spatiotemporal dynamics. AKFED leverages MODIS active fire data to assign daily burned area and the FRP and active fire approaches essentially redistribute the total

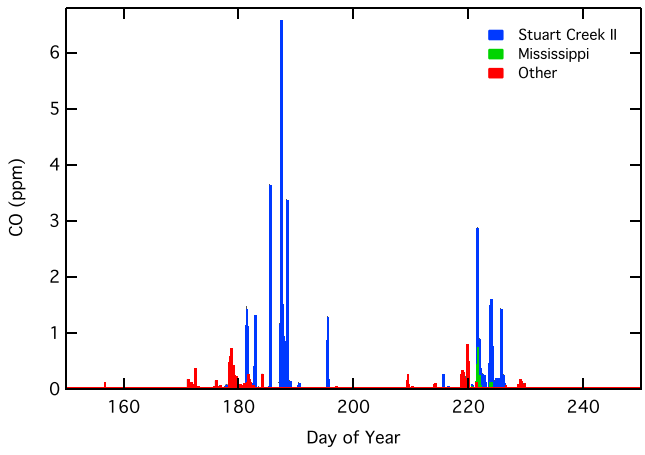

Figure 9. Contributions to CO (ppm) observed at the CRV tower from individual fire events. The Stuart Creek II fire is shown in blue, the Mississippi fire in green, and the sum of other fires is shown in red.

carbon emissions from AKFED in space and time based on the timing and locations of the MODIS active fire detections. Daily variability in AKFED is primarily driven by variations in burned area with a smaller influence of differences in carbon consumption. Likewise, the number of active fires and burned area is highly correlated [*Giglio et al*., 2003], highlighting another shared characteristic of the different emissions time series.

5. Conclusions

By combining a high-resolution fire emissions inventory with a regional atmospheric model, we estimated fire contributions to trace gas variability measured at a tower in interior Alaska. Our modeling system enabled us to isolate the contribution of individual fires to daily variations in trace gas mole fractions and was uniquely constrained by region-specific emission factors and injection height information. We found moderate levels of correlation between observed and modeled CO, CH_4, and CO_2 concentrations from boreal fires. Differences between modeled and observed atmospheric mole fractions can be explained by underlying uncertainties in the emissions inventory, transport modeling system, and our assumptions regarding the use of fixed emission factor and plume injection parameterizations. VPD and temperature variables had a similar level of correlation with daily fire time series as more complex Canadian forest fire weather indexes, including FWI. We found emission factors that were above average relative to the mean of previous studies. Further study of high-resolution CO, CH_4, and CO_2 tower measurements during a high fire year using this method could provide opportunities to estimate boreal forest fire emission ratios. Our analysis demonstrates the feasibility of combining high-resolution fire emissions and atmospheric transport models to study relationships between meteorology and emissions. Further work building on this approach may further reduce uncertainties of fire-climate feedbacks in the boreal forest.

Acknowledgments
The research described in this paper was performed for the Carbon in Arctic Reservoirs Vulnerability Experiment (CARVE), an Earth Ventures (EV-S1) investigation, under contract with the National Aeronautics and Space Administration. E.B.W. thanks the U.S. National Science Foundation for a Graduate Research Fellowship (NSF 2013172241). Computing resources for this work were provided by the NASA High-End Computing (HEC) Program through the NASA Advanced Supercomputing (NAS) Division at Ames Research Center. The meteorological data used in this study are publicly available found online from the National Climatic Data Center (http://www7.ncdc.noaa.gov/CDO/cdopoe-main.cmd). The CRV tower observations used in our analysis are archived at the U.S. Oak Ridge National Laboratory Distributed Active Archive Center for Biogeochemical Dynamics (http://dx.doi.org/10.3334/ORNLDAAC/1316). The MISR data were obtained from the NASA Langley Research Center Atmospheric Science Data Center and can be acquired online using the MISR Order and Customization Tool (http://l0dup05.larc.nasa.gov/MISR/cgi-bin/MISR/main.cgi).

References

Abatzoglou, J. T., and C. A. Kolden (2011), Relative importance of weather and climate on wildfire growth in interior Alaska, *Int. J. Wildland Fire*, *20*(4), 479–486.

Akagi, S., R. J. Yokelson, C. Wiedinmyer, M. Alvarado, J. Reid, T. Karl, J. Crounse, and P. Wennberg (2011), Emission factors for open and domestic biomass burning for use in atmospheric models, *Atmos. Chem. Phys.*, *11*(9), 4039–4072.

Alexander, M. E. (1982), Calculating and interpreting forest fire intensities, *Can. J. Bot.*, *60*(4), 349–357.

Amiro, B., A. Orchansky, A. Barr, T. Black, S. Chambers, F. Chapin III, M. Goulden, M. Litvak, H. Liu, and J. McCaughey (2006), The effect of post-fire stand age on the boreal forest energy balance, *Agric. For. Meteorol.*, *140*(1), 41–50.

Anderson, K. (2002), A model to predict lightning-caused fire occurrences, *Int. J. Wildland Fire*, *11*(4), 163–172.

Anderson, K., B. Simpson, R. J. Hall, P. Englefield, M. Gartrell, and J. M. Metsaranta (2015), Integrating forest fuels and land cover data for improved estimation of fuel consumption and carbon emissions from boreal fires, *Int. J. Wildland Fire*, *24*(5), 665–679.

Apps, M., W. Kurz, R. Luxmoore, L. Nilsson, R. Sedjo, R. Schmidt, L. Simpson, and T. Vinson (1993), Boreal forests and tundra, *Water Air Soil Pollut.*, *70*(1–4), 39–53.

Bedia, J., S. Herrera, J. M. Gutiérrez, A. Benali, S. Brands, B. Mota, and J. M. Moreno (2015), Global patterns in the sensitivity of burned area to fire-weather: Implications for climate change, *Agric. For. Meteorol.*, *214*, 369–379.

Bergeron, Y., M. Flannigan, S. Gauthier, A. Leduc, and P. Lefort (2004), Past, current and future fire frequency in the Canadian boreal forest: Implications for sustainable forest management, *Ambio*, *33*(6), 356–360.

Bessie, W., and E. Johnson (1995), The relative importance of fuels and weather on fire behavior in subalpine forests, *Ecology*, *76*(3), 747–762.

Boby, L. A., E. A. Schuur, M. C. Mack, D. Verbyla, and J. F. Johnstone (2010), Quantifying fire severity, carbon, and nitrogen emissions in Alaska's boreal forest, *Ecol. Appl.*, *20*(6), 1633–1647.

Chang, R. Y. W., et al. (2014), Methane emissions from Alaska in 2012 from CARVE airborne observations, *Proc. Natl. Acad. Sci. U.S.A.*, *111*(47), 16,694–16,699.

Chen, H., A. Karion, C. W. Rella, J. Winderlich, C. Gerbig, A. Filges, T. Newberger, C. Sweeney, and P. P. Tans (2013), Accurate measurements of carbon monoxide in humid air using the cavity ring-down spectroscopy (CRDS) technique, *Atmos. Meas. Tech.*, *6*(4), 1031–1040.

Cofer, W., E. Winstead, B. Stocks, J. Goldammer, and D. Cahoon (1998), Crown fire emissions of CO_2, CO, H_2, CH_4, and TNMHC from a dense jack pine boreal forest fire, *Geophys. Res. Lett.*, *25*, 3919–3922, doi:10.1029/1998GL900042.

Duck, T. J., et al. (2007), Transport of forest fire emissions from Alaska and the Yukon Territory to Nova Scotia during summer 2004, *J. Geophys. Res.*, *112*, D10S44, doi:10.1029/2006JD007716.

Duffy, P. A., J. E. Walsh, J. M. Graham, D. H. Mann, and T. S. Rupp (2005), Impacts of large-scale atmospheric-ocean variability on Alaskan fire season severity, *Ecol. Appl.*, *15*(4), 1317–1330.

Flanner, M. G., C. S. Zender, J. T. Randerson, and P. J. Rasch (2007), Present day climate forcing and response from black carbon in snow, *J. Geophys. Res.*, *112*, D11202, doi:10.1029/2006JD008003.

Flannigan, M., I. Campbell, M. Wotton, C. Carcaillet, P. Richard, and Y. Bergeron (2001), Future fire in Canada's boreal forest: Paleoecology results and general circulation model-regional climate model simulations, *Can. J. For. Res.*, *31*(5), 854–864.

Flannigan, M. D., and J. Harrington (1988), A study of the relation of meteorological variables to monthly provincial area burned by wildfire in Canada (1953–80), *J. Appl. Meteorol.*, *27*(4), 441–452.

Freitas, S. R., K. M. Longo, M. A. F. Silva Dias, R. Chatfield, P. Silva Dias, P. Artaxo, and J. Panetta (2009), The coupled aerosol and tracer transport model to the Brazilian developments on the regional atmospheric modeling system (CATT-BRAMS)–part 1: Model description and evaluation, *Atmos. Chem. Phys.*, *9*(8), 2843–2861.

French, N. H., E. S. Kasischke, and D. G. Williams (2002), Variability in the emission of carbon based trace gases from wildfire in the Alaskan boreal forest, *J. Geophys. Res.*, *107*, 8151, doi:10.1029/2001JD000480. [Printed *108*(D1), 2003.]

French, N. H., P. Goovaerts, and E. S. Kasischke (2004), Uncertainty in estimating carbon emissions from boreal forest fires, *J. Geophys. Res.*, *109*, D14S08, doi:10.1029/2003JD003635.

French, N. H., D. McKenzie, T. Erickson, B. Koziol, M. Billmire, K. A. Endsley, N. K. Yager Scheinerman, L. Jenkins, M. E. Miller, and R. Ottmar (2014), Modeling regional-scale wildland fire emissions with the Wildland Fire Emissions Information System, *Earth Interact.*, *18*(16), 1–26, doi:10.1175/EI-D-14-0002.1.

Giglio, L., J. Descloitres, C. O. Justice, and Y. J. Kaufman (2003), An enhanced contextual fire detection algorithm for MODIS, *Remote Sens. Environ.*, *87*(2), 273–282.

Goode, J. G., R. J. Yokelson, D. E. Ward, R. A. Susott, R. E. Babbitt, M. A. Davies, and W. M. Hao (2000), Measurements of excess O_3, CO_2, CO, CH_4, C_2H_4, C_2H_2, HCN, NO, NH_3, HCOOH, CH_3COOH, HCHO, and CH_3OH in 1997 Alaskan biomass burning plumes by airborne Fourier transform infrared spectroscopy (AFTIR), *J. Geophys. Res.*, *105*, 22,147–22,166, doi:10.1029/2000JD900287.

Grell, G., S. Freitas, M. Stuefer, and J. Fast (2011), Inclusion of biomass burning in WRF-Chem: Impact of wildfires on weather forecasts, *Atmos. Chem. Phys.*, *11*, 5289–5303.

Harden, J. W., S. Trumbore, B. Stocks, A. Hirsch, S. Gower, K. O'neill, and E. Kasischke (2000), The role of fire in the boreal carbon budget, *Global Change Biol.*, *6*(S1), 174–184.

Henderson, J., J. Eluszkiewicz, M. Mountain, T. Nehrkorn, R. W. Chang, A. Karion, J. Miller, C. Sweeney, N. Steiner, and S. Wofsy (2015), Atmospheric transport simulations in support of the Carbon in Arctic Reservoirs Vulnerability Experiment (CARVE), *Atmos. Chem. Phys.*, *15*, 4093–4116.

Hobbie, S. E., J. P. Schimel, S. E. Trumbore, and J. T. Randerson (2000), Controls over carbon storage and turnover in high-latitude soils, *Global Change Biol.*, *6*(S1), 196–210.

Ichoku, C., and Y. J. Kaufman (2005), A method to derive smoke emission rates from MODIS fire radiative energy measurements, *IEEE Trans. Geosci. Remote Sens.*, *43*(11), 2636–2649.

Johnson, E. A. (1996), *Fire and Vegetation Dynamics: Studies From the North American Boreal Forest*, pp. 3–11, Cambridge Univ. Press, Cambridge, U. K.

Johnstone, J. F., and F. S. Chapin III (2006), Effects of soil burn severity on post-fire tree recruitment in boreal forest, *Ecosystems*, *9*(1), 14–31.

Johnstone, J. F., F. Chapin Iii, J. Foote, S. Kemmett, K. Price, and L. Viereck (2004), Decadal observations of tree regeneration following fire in boreal forests, *Can. J. For. Res.*, *34*(2), 267–273.

Jordan, N. S., C. Ichoku, and R. M. Hoff (2008), Estimating smoke emissions over the US Southern Great Plains using MODIS fire radiative power and aerosol observations, *Atmos. Environ.*, *42*(9), 2007–2022.

Kahn, R. A., Y. Chen, D. L. Nelson, F. Y. Leung, Q. B. Li, D. J. Diner, and J. A. Logan (2008), Wildfire smoke injection heights: Two perspectives from space, *Geophys. Res. Lett.*, *35*, L04809, doi:10.1029/2007GL032165.

Kaiser, J., M. Suttie, J. Flemming, J. Morcrette, O. Boucher, and M. Schultz (2009), Global real-time fire emission estimates based on space-borne fire radiative power observations, *Curr. Probl. Atmos. Radiat.*, *1100*, 645–648.

Karion, A., et al. (2016a), Investigating Alaskan methane and carbon dioxide fluxes using measurements from the CARVE tower, *Atmos. Chem. Phys.*, *16*(8), 5383–5398.

Karion, A., et al. (2016b), *CARVE: CH_4, CO_2, and CO Atmospheric Concentrations, CARVE Tower, Alaska, 2012–2014*, ORNL DAAC, Oak Ridge, Tenn., doi:10.3334/ORNLDAAC/1316.

Kasischke, E. S., N. Christensen Jr., and B. J. Stocks (1995), Fire, global warming, and the carbon balance of boreal forests, *Ecol. Appl.*, *5*(2), 437–451.

Kasischke, E. S., E. J. Hyer, P. C. Novelli, L. P. Bruhwiler, N. H. F. French, A. I. Sukhinin, J. H. Hewson, and B. J. Stocks (2005), Influences of boreal fire emissions on Northern Hemisphere atmospheric carbon and carbon monoxide, *Global Biogeochem. Cycles*, *19*, GB1012, doi:10.1029/2004GB002300.

Larkin, N. K., S. M. O'Neill, R. Solomon, S. Raffuse, T. Strand, D. C. Sullivan, and S. A. Ferguson (2010), The BlueSky smoke modeling framework, *Int. J. Wildland Fire*, *18*(8), 906–920.

Latham, D. J., and J. A. Schlieter (1989), Ignition probabilities of wildland fuels based on simulated lightning discharges, U.S. Dep. of Agric., For. Serv., Intermountain Res. Station.

Lawrence, M. G. (2005), The relationship between relative humidity and the dewpoint temperature in moist air: A simple conversion and applications, *Bull. Am. Meteorol. Soc.*, *86*(2), 225–233.

Lawson, D. E. (1986), Response of permafrost terrain to disturbance: A synthesis of observations from northern Alaska, USA, *Arct. Alp. Res.*, *18*(1), 1–17.

Leung, F. Y. T., J. A. Logan, R. Park, E. Hyer, E. Kasischke, D. Streets, and L. Yurganov (2007), Impacts of enhanced biomass burning in the boreal forests in 1998 on tropospheric chemistry and the sensitivity of model results to the injection height of emissions, *J. Geophys. Res.*, *112*, D10313, doi:10.1029/2006JD008132.

Lin, J., C. Gerbig, S. Wofsy, V. Chow, E. Gottlieb, B. Daube, and D. Matross (2007), Designing Lagrangian experiments to measure regional scale trace gas fluxes, *J. Geophys. Res.*, *112*, D13312, doi:10.1029/2006JD008077.

Longo, K., S. R. Freitas, A. Setzer, E. Prins, P. Artaxo, and M. Andreae (2007), The Coupled Aerosol and Tracer Transport model to the Brazilian developments on the Regional Atmospheric Modeling System (CATT-BRAMS). Part 2: Model sensitivity to the biomass burning inventories, *Atmos. Chem. Phys. Discuss.*, *7*(3), 8571–8595.

Luus, K., and J. Lin (2015), The Polar Vegetation Photosynthesis and Respiration Model (PolarVPRM): A parsimonious, satellite data-driven model of high-latitude CO_2 exchange, *Geosci. Model Dev.*, *8*, 2655–2674, doi:10.5194/gmd-8-2655-2015.

Martin, M. V., R. E. Honrath, R. C. Owen, G. Pfister, P. Fialho, and F. Barata (2006), Significant enhancements of nitrogen oxides, black carbon, and ozone in the North Atlantic lower free troposphere resulting from North American boreal wildfires, *J. Geophys. Res.*, *111*, D23S60, doi:10.1029/2006JD007530.

McGuire, A. D., R. W. Macdonald, E. A. Schuur, J. W. Harden, P. Kuhry, D. J. Hayes, T. R. Christensen, and M. Heimann (2010), The carbon budget of the northern cryosphere region, *Curr. Opin. Environ. Sustainability*, *2*(4), 231–236.

Mu, M., et al. (2011), Daily and 3-hourly variability in global fire emissions and consequences for atmospheric model predictions of carbon monoxide, *J. Geophys. Res.*, *116*, D24303, doi:10.1029/2011JD016245.

Nance, J. D., P. V. Hobbs, L. F. Radke, and D. E. Ward (1993), Airborne measurements of gases and particles from an Alaskan wildfire, *J. Geophys. Res.*, *98*, 14,873–14,882, doi:10.1029/93JD01196.

Nash, C., and E. Johnson (1996), Synoptic climatology of lightning-caused forest fires in subalpine and boreal forests, *Can. J. For. Res.*, *26*(10), 1859–1874.

Nehrkorn, T., J. Henderson, M. Leidner, M. Mountain, J. Eluszkiewicz, K. McKain, and S. Wofsy (2013), WRF simulations of the urban circulation in the Salt Lake City area for CO_2 modeling, *J. Appl. Meteorol. Climatol.*, *52*(2), 323–340.

Nelson, D. L., M. J. Garay, R. A. Kahn, and B. A. Dunst (2013), Stereoscopic height and wind retrievals for aerosol plumes with the MISR INteractive eXplorer (MINX), *Remote Sens.*, *5*(9), 4593–4628.

Pavlovic, R., J. Chen, K. Anderson, M. D. Moran, P. A. Beaulieu, D. Davignon, and S. Cousineau (2016), The FireWork air quality forecast system with near-real-time biomass burning emissions: Recent developments and evaluation of performance for the 2015 North American wildfire season, *J. Air Waste Manage.*, *66*, 819–841.

Pechony, O., and D. Shindell (2009), Fire parameterization on a global scale, *J. Geophys. Res.*, *114*, D16115, doi:10.1029/2009JD011927.

Preston, C., and M. Schmidt (2006), Black (pyrogenic) carbon: A synthesis of current knowledge and uncertainties with special consideration of boreal regions, *Biogeosciences*, *3*(4), 397–420.

Radke, L. F., D. A. Hegg, P. V. Hobbs, J. D. Nance, J. H. Lyons, K. K. Laursen, R. E. Weiss, P. J. Riggan, and D. E. Ward (1991), Particulate and trace gas emissions from large biomass fires in North America, in *Global Biomass Burning: Atmospheric, Climatic, and Biospheric Implications*, edited by J. S. Levine, pp. 209–224, MIT Press, Cambridge, Mass.

Rapalee, G., S. E. Trumbore, E. A. Davidson, J. W. Harden, and H. Veldhuis (1998), Soil carbon stocks and their rates of accumulation and loss in a boreal forest landscape, *Global Biogeochem. Cycles*, *12*, 687–701, doi:10.1029/98GB02336.

Reichle, R. H., R. D. Koster, G. J. M. De Lannoy, B. A. Forman, Q. Liu, S. P. P. Mahanama, and A. Touré (2011), Assessment and enhancement of MERRA land surface hydrology estimates, *J. Clim.*, *24*(24), 6322–6338.

Rella, C. W., H. Chen, A. E. Andrews, A. Filges, C. Gerbig, J. Hatakka, and C. Sweeney (2013), High accuracy measurements of dry mole fractions of carbon dioxide and methane in humid air, *Atmos. Meas. Tech.*, *6*(3), 837–860.

Rogers, B. M., J. T. Randerson, and G. B. Bonan (2013), High latitude cooling associated with landscape changes from North American boreal forest fires, *Biogeosciences*, *10*(2), 699–718.

Rogers, B. M., A. J. Soja, M. L. Goulden, and J. T. Randerson (2015), Influence of tree species on continental differences in boreal fires and climate feedbacks, *Nat. Geosci.*, *8*(3), 228–234.

Sedano, F., and J. Randerson (2014), Multi-scale influence of vapor pressure deficit on fire ignition and spread in boreal forest ecosystems, *Biogeosciences*, *11*(14), 3739–3755.

Seiler, W., and P. J. Crutzen (1980), Estimates of gross and net fluxes of carbon between the biosphere and the atmosphere from biomass burning, *Clim. Change*, *2*(3), 207–247.

Simpson, I. J., S. Akagi, B. Barletta, N. Blake, Y. Choi, G. Diskin, A. Fried, H. Fuelberg, S. Meinardi, and F. Rowland (2011), Boreal forest fire emissions in fresh Canadian smoke plumes: C_1–C_{10} volatile organic compounds (VOCs), CO_2, CO, NO_2, NO, HCN and CH_3CN, *Atmos. Chem. Phys.*, *11*(13), 6445–6463.

Skamarock, W. C., J. B. Klemp, J. Dudhia, D. O. Gill, D. M. Barker, W. Wang, and J. G. Powers (2005), A description of the Advanced WRF Version 2, Tech. Note NCAR/TN-468+ STR, Natl. Cent. for Atmos. Res., Boulder, Colo.

Stocks, B. J., M. Fosberg, T. Lynham, L. Mearns, B. Wotton, Q. Yang, J. Jin, K. Lawrence, G. Hartley, and J. Mason (1998), Climate change and forest fire potential in Russian and Canadian boreal forests, *Clim. Change*, *38*(1), 1–13.

Tetens, O. (1930), Uber einige meteorologische Begriffe, *Z. Geophys.*, *6*, 297–309.

Trumbore, S. E., and J. Harden (1997), Accumulation and turnover of carbon in organic and mineral soils of the BOREAS northern study area, *J. Geophys. Res.*, *102*, 28,817–28,830, doi:10.1029/97JD02231.

Turetsky, M. R., E. S. Kane, J. W. Harden, R. D. Ottmar, K. L. Manies, E. Hoy, and E. S. Kasischke (2011), Recent acceleration of biomass burning and carbon losses in Alaskan forests and peatlands, *Nat. Geosci.*, *4*(1), 27–31.

Turetsky, M. R., B. Benscoter, S. Page, G. Rein, G. R. van der Werf, and A. Watts (2015), Global vulnerability of peatlands to fire and carbon loss, *Nat. Geosci.*, *8*(1), 11–14.

Turquety, S., et al. (2007), Inventory of boreal fire emissions for North America in 2004: Importance of peat burning and pyroconvective injection, *J. Geophys. Res.*, *112*, D12S03, doi:10.1029/2006JD007281.

van der Werf, G. R., J. T. Randerson, L. Giglio, G. J. Collatz, P. S. Kasibhatla, and A. F. Arellano Jr. (2006), Interannual variability in global biomass burning emissions from 1997 to 2004, *Atmos. Chem. Phys.*, *6*(11), 3423–3441.

van der Werf, G. R., J. T. Randerson, L. Giglio, G. Collatz, M. Mu, P. S. Kasibhatla, D. C. Morton, R. DeFries, Y. Jin, and T. T. van Leeuwen (2010), Global fire emissions and the contribution of deforestation, savanna, forest, agricultural, and peat fires (1997–2009), *Atmos. Chem. Phys.*, *10*(23), 11,707–11,735.

Van Wagner, C. E. (1987), The development and structure of the Canadian forest fire weather index system, *For. Tech. Rep. 35*, 37 pp., Can. For. Serv., Ottawa, Ont.

Veraverbeke, S., B. Rogers, and J. Randerson (2015), Daily burned area and carbon emissions from boreal fires in Alaska, *Biogeosciences*, *12*(11), 3579–3601.

Viereck, L. A., R. Wein, and D. Maclean (1983), The effects of fire in black spruce ecosystems of Alaska and northern Canada, in *The Role of Fire in Northern Circumpolar Ecosystems*, edited by R. W. Wein and D. A. MacLellan, pp. 201–220, John Wiley, New York.

Wiedinmyer, C., S. K. Akagi, R. J. Yokelson, L. K. Emmons, J. A. Al-Saadi, J. J. Orlando, and A. J. Soja (2011), The Fire INventory from NCAR (FINN): A high resolution global model to estimate the emissions from open burning, *Geosci. Model Dev.*, *4*(3), 625–641.

Wirth, C., E. D. Schulze, W. Schulze, D. von Stünzner-Karbe, W. Ziegler, I. Miljukova, A. Sogatchev, A. Varlagin, M. Panvyorov, and S. Grigoriev (1999), Above-ground biomass and structure of pristine Siberian Scots pine forests as controlled by competition and fire, *Oecologia*, *121*(1), 66–80.

Wooster, M. J., G. Roberts, G. Perry, and Y. Kaufman (2005), Retrieval of biomass combustion rates and totals from fire radiative power observations: FRP derivation and calibration relationships between biomass consumption and fire radiative energy release, *J. Geophys. Res.*, *110*, D24311, doi:10.1029/2005JD006318.

Yokelson, R. J., R. Susott, D. E. Ward, J. Reardon, and D. W. Griffith (1997), Emissions from smoldering combustion of biomass measured by open path Fourier transform infrared spectroscopy, *J. Geophys. Res.*, *102*, 18,865–18,877, doi:10.1029/97JD00852.